

福昕PDF编辑器

• 永久 • 轻巧 • 自由

升级会员

批量购买



永久使用

无限制使用次数



极速轻巧

超低资源占用，告别卡顿慢



自由编辑

享受Word一样的编辑自由



扫一扫，关注公众号

Infrared Small Target Detection Utilizing the Multiscale Relative Local Contrast Measure

Jinhui Han, Kun Liang^{ID}, Bo Zhou^{ID}, Xinying Zhu, Jie Zhao, and Linlin Zhao

Abstract—Infrared (IR) small target detection with high detection rate, low false alarm rate, and high detection speed has a significant value, but it is usually very difficult since the small targets are usually very dim and may be easily drowned in different types of interferences. Current algorithms cannot effectively enhance real targets and suppress all the types of interferences simultaneously. In this letter, a multiscale detection algorithm utilizing the relative local contrast measure (RLCM) is proposed. It has a simple structure: first, the multiscale RLCM is calculated for each pixel of the raw IR image to enhance real targets and suppress all the types of interferences simultaneously; then, an adaptive threshold is applied to extract real targets. Experimental results show that the proposed algorithm can deal with different sizes of small targets under complex backgrounds and has a better effectiveness and robustness against existing algorithms. Besides, the proposed algorithm has the potential of parallel processing, which is very useful for improving the detection speed.

Index Terms—Human visual system (HVS), infrared (IR) small target, multiscale detection, relative local contrast measure (RLCM).

I. INTRODUCTION

INFRARED (IR) small target detection plays an important role in precise guidance and early warning [1], [2]. However, it is usually very difficult to detect IR small target with high detection rate, low false alarm rate, and high speed because of the following facts.

- 1) Due to the long distance between the target and the detector, the target usually has a dim gray level in the raw IR image [3].
- 2) There are usually different types of interferences in the raw IR image, such as high brightness backgrounds, complex background edges, and pixel-sized noises with high brightness (PNHB) [4].
- 3) The target size is usually unknown in real applications, so multiscale detection is usually needed [5].

In recent years, the detection algorithms based on robust human visual system (HVS) properties have been widely

Manuscript received July 30, 2017; revised October 18, 2017 and December 7, 2017; accepted December 27, 2017. Date of publication February 12, 2018; date of current version March 23, 2018. This work was supported in part by the Aero Science Foundation of China Project under Grant 20160179001, in part by the Foundation of the Education Department of Henan Province under Grant 18B510021, and in part by the Start-up Research of Zhoukou Normal University under Grant ZKNUC2016017. (*Corresponding author: Kun Liang*)

J. Han, X. Zhu, J. Zhao, and L. Zhao are with the College of Physics and Telecommunication Engineering, Zhoukou Normal University, Zhoukou 466001, China (e-mail: hanjinhui@zknu.edu.cn; zxinying0824@126.com; zhaojie@zknu.edu.cn; me_zhaolinlin@163.com).

K. Liang and B. Zhou are with the School of Electronic Information and Communications, Huazhong University of Science and Technology, Wuhan 430074, China (e-mail: liangkun@hust.edu.cn; zhoub@hust.edu.cn).

Color versions of one or more of the figures in this letter are available online at <http://ieeexplore.ieee.org>.

Digital Object Identifier 10.1109/LGRS.2018.2790909

studied; they can usually achieve better detection performances than traditional algorithms, since they extract targets according to the local contrast rather than the brightness [4]–[12]. However, how to calculate the local contrast is one of the key issues for an algorithm based on HVS, which directly determines the detection performance.

Until now, consensus on how to calculate the local contrast has not been reached, and different researchers tend to use different local contrast definitions. Current definitions can be generally divided into two categories: the difference form definitions and the ratio form definitions. The difference form definitions, including the Laplacian of Gaussian (LoG) filter [5], the difference of Gaussian (DoG) filter [6], the improved difference of Gabor filter [7], the accumulated center-surround difference measure [8], and the multiscale patch-based contrast measure (MPCM) [9], take the difference between the local center and the local surrounding as the local contrast. These algorithms can effectively eliminate the high brightness backgrounds; however, they cannot effectively enhance the small targets.

The ratio form definitions, including the local contrast measure (LCM) [10], the improved local contrast measure (ILCM) [4], the novel local contrast measure (NLCM) [11], and the weighted local difference measure (WLDM) [12], first calculate the ratio between the local center and the local surrounding as an enhancement factor, then take the product of the enhancement factor and the local center value as the local contrast. These algorithms can effectively enhance targets; however, they use the absolute local contrast and cannot effectively eliminate high brightness backgrounds. An improvement is to combine with a preprocessing such as DoG or LoG [4], [11]. However, the detection robustness may be damaged since any error in any algorithm will jam the result.

In this letter, an IR small dim target detection algorithm utilizing the multiscale relative local contrast measure (RLCM) is proposed. It can deal with different sizes of small targets effectively under complex backgrounds, and does not need a preprocessing algorithm to eliminate high brightness backgrounds, so its robustness can be guaranteed. Besides, the proposed algorithm has the potential of parallel processing, which is very useful for improving the detection speed.

II. PROPOSED ALGORITHM

The flowchart of the proposed algorithm is shown in Fig. 1. It has a simple structure: first, the multiscale RLCM is calculated for each pixel of the raw IR image to enhance real targets and suppress all the types of interferences simultaneously (including high brightness backgrounds, complex background edges, and PNHB); then, an adaptive threshold is applied to extract real targets.

A. RLCM Calculation

In this letter, inspired by LCM [10], we use the nine-cell image patch window (shown in the top-left corner of Fig. 1,

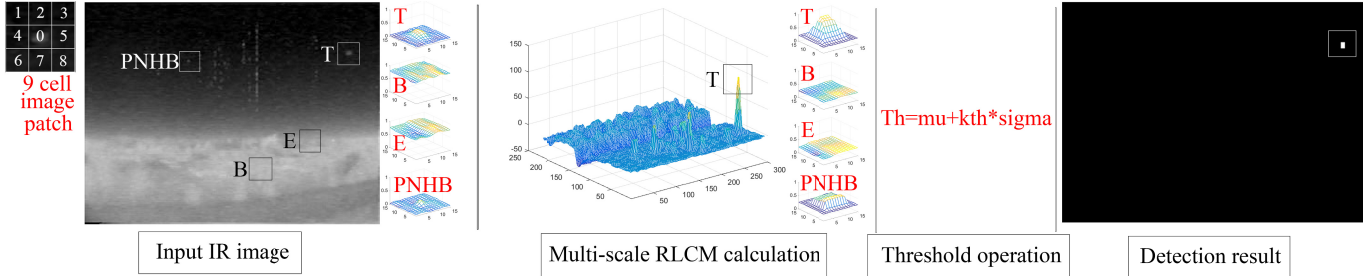


Fig. 1. Flowchart of the proposed algorithm.

the cell size should be close to or slightly larger than targets) to calculate the RLCM for each pixel of the raw IR image, i.e., slide the image patch window from left to right and top to bottom pixel by pixel on the raw image; at each location, the RLCM of the central pixel of the central cell is defined as

$$\begin{aligned} \text{RLCM} &= \min \left(\frac{I_{\text{mean}_0}}{I_{\text{mean}_i}} I_{\text{mean}_0} - I_{\text{mean}_0} \right) \\ &= \min(f_i I_{\text{mean}_0} - I_{\text{mean}_0}), \quad i = 1, 2, \dots, 8 \end{aligned} \quad (1)$$

where the f_i can be understood as an enhancement factor for the central cell [i.e., cell(0)] in the i th direction, I_{mean_0} or I_{mean_i} denotes the average gray of the K_1 or K_2 max pixels in cell(0) or cell(i), shown in the following equations:

$$I_{\text{mean}_0} = \frac{1}{K_1} \sum_{j=1}^{K_1} G_0^j \quad (2)$$

$$I_{\text{mean}_i} = \frac{1}{K_2} \sum_{j=1}^{K_2} G_i^j, \quad i = 1, 2, \dots, 8 \quad (3)$$

where K_1 and K_2 are the numbers of maximal gray values considered, and G_0^j or G_i^j is the j th maximal gray value of cell(0) or cell(i). To get a larger f_i , it is suggested to set K_2 to a value slightly larger than K_1 .

As shown in Fig. 1, there are usually different types of interferences in the raw image, such as high brightness backgrounds, complex background edges, and PNHB. We will discuss the RLCM results for different types of pixels.

- 1) For a target pixel (denoted by T), since real small targets are usually locally salient, we can easily get

$$f_i > 1, \quad i = 1, 2, \dots, 8 \quad (4)$$

$$\text{RLCM}_T > 0. \quad (5)$$

- 2) For a background pixel (denoted by B), since backgrounds are usually large and continuous, we can easily get

$$f_i \approx 1, \quad i = 1, 2, \dots, 8 \quad (6)$$

$$\text{RLCM}_B \approx 0. \quad (7)$$

Comparing (5) with (7), it can be seen that the small targets can be enhanced while the backgrounds (including high brightness backgrounds) are discarded using RLCM. In fact, the RLCM can be understood as the difference between the enhanced cell(0) and the original cell(0) according to (1), that is why it is named as RLCM. The benefit of the difference operation is that it can eliminate the high brightness backgrounds effectively, so no preprocessing algorithm such as DoG or LoG is needed.

3) For a background edge pixel (denoted by E), since background edges usually distribute along a particular direction in a local small area, the minimum operation for different directions in (1) ensures that the RLCM can suppress complex background edges effectively, and there will be

$$\text{RLCM}_E \leq 0. \quad (8)$$

4) For a PNHB, even its gray value is close to or slightly larger than real target, and its I_{mean_0} will be still smaller than a real target's when we set K_1 to a value larger than 1, so

$$\text{RLCM}_T > \text{RLCM}_{\text{PNHB}}. \quad (9)$$

From the discussions above, we can get the conclusion that after RLCM calculation, true small targets will be the most salient, and all the types of interferences will be suppressed.

B. Multiscale RLCM Calculation

The K_1 and K_2 in (2) and (3) are two key parameters in the proposed algorithm. To achieve a better enhancement on real small targets, K_1 and K_2 need to be automatically adjusted according to the target size. However, target size is usually unknown in practice, which means that multiscale RLCM calculation will be needed. The proceedings of multiscale RLCM calculation are shown as follows.

- 1) For the s th scale ($s = 1, 2, \dots, L$, where L is the number of scales been used), select the proper K_{1s} and K_{2s} .
- 2) For a given IR image, calculate the RLCM_s according to (1) using K_{1s} and K_{2s} ($s = 1, 2, \dots, L$).
- 3) For each pixel, output the maximum value of different scales as the final result, and form them as a saliency map (SM)

$$\text{SM}(i, j) = \max(\text{RLCM}_s(i, j)), \quad s = 1, 2, \dots, L \quad (10)$$

where (i, j) is the coordinate of each pixel.

It can be easily proved that after the multiscale RLCM calculation, the conclusions in (5) and (7)–(9) are still true. Besides, the proposed algorithm has the potential of parallel processing, which is very useful for improving the detection speed: the calculations for different scales can be carried out in parallel; for each scale, the calculations for different pixels can be carried out in parallel; and for each pixel, the calculations for different directions can be carried out in parallel.

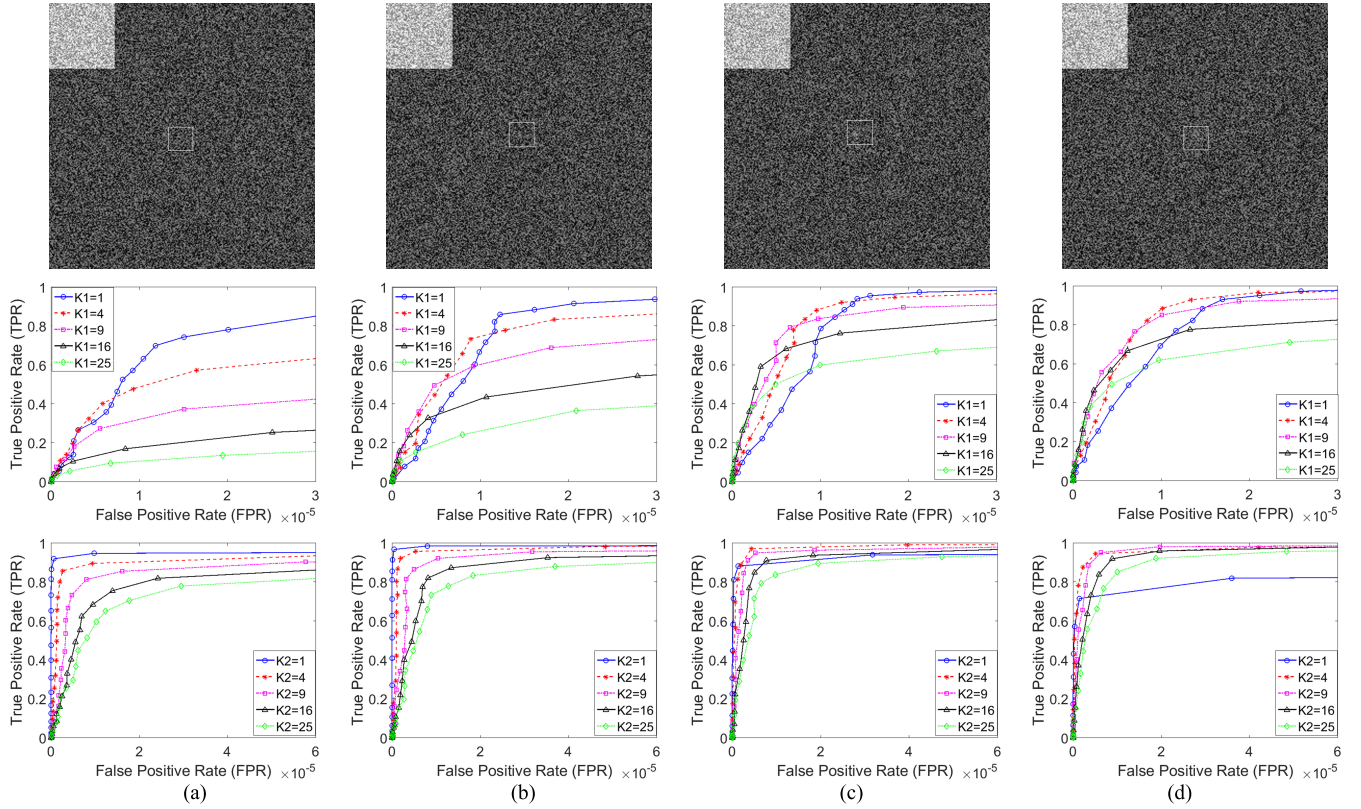


Fig. 2. (Top) Simulated images with different target sizes. (a) 3×3 target. (b) 5×5 target. (c) 7×7 target. (d) 9×9 target. (Middle) ROC curves of different K_1 for different target sizes when K_2 is constant 25. (Bottom) ROC curves of different K_2 when K_1 is constant [2 for (a), 4 for (b), and 9 for (c) and (d)].

C. Threshold Operation

In SM, true small targets will be the most salient; they can be extracted by a threshold operation. In this letter, the threshold Th is adaptively defined as

$$Th = \mu_{SM} + k_{th} \times \sigma_{SM} \quad (11)$$

where μ_{SM} and σ_{SM} are the mean and standard deviation of SM, and k_{th} is a given parameter. Our experiments show that the optimal range of k_{th} is from 2 to 9.

The pixels which have larger RLCM value than Th will be output as target pixels, while other parts are discarded.

III. SIMULATIONS AND EXPERIMENTAL RESULTS

In this section, a large number of simulations and experiments had been done to choose the optimal key parameters, including K_1 , K_2 , and the cell size N . Then, detection results and comparisons with other state-of-the-art algorithms on three real IR sequences would be given. All the simulations and experiments were conducted on a computer with 8-GB memory and 2.6-GHz Intel i5 processor, and the code was implemented in MATLAB R2016b.

A. Choice of K_1 , K_2 , and N

K_1 and K_2 in (2) and (3) are two key parameters which determine the detection performance directly. In this letter, for different target sizes, numerous simulations had been done to choose the optimal K_1 and K_2 . The resolution of the simulated images was set to 256×256 . The brightness of normal background was set to 100; in particular, in the top-left corner, there was a small area (64×64) of high brightness background with a gray value of 200. The target was located at (128, 128);

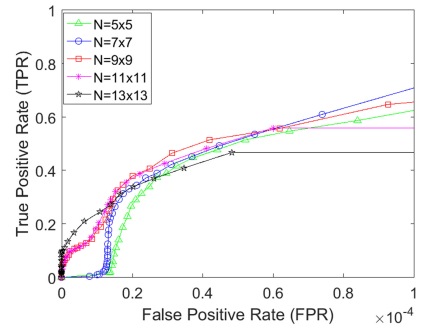


Fig. 3. ROC curves of Seq. 1 for different N .

in this letter, we used the 2-D Gaussian model to generate the small target [13], the maximum gray value of the target was set to 120, and different target sizes including 3×3 , 5×5 , 7×7 , and 9×9 were tested; for each target size, 1000 images were generated. Random noises with a gray value of 0–125 were added to each simulated image. Samples of the simulated images for different target sizes are shown in Fig. 2 (top).

First, we set K_2 to a constant value of 25, and tested different K_1 ; in this letter, $K_1 = 1, 4, 9, 16, 25$ were tested. The receiver operating characteristic (ROC) curves [14] for each target size are given in Fig. 2 (middle), where the false positive rate (FPR) and the true positive rate (TPR) are defined as (12) and (13). The cell size N is set to 9×9 here

$$FPR = \frac{\text{number of detected false targets}}{\text{total number of pixels in the whole image}} \quad (12)$$

$$TPR = \frac{\text{number of detected true targets}}{\text{total number of real targets}}. \quad (13)$$

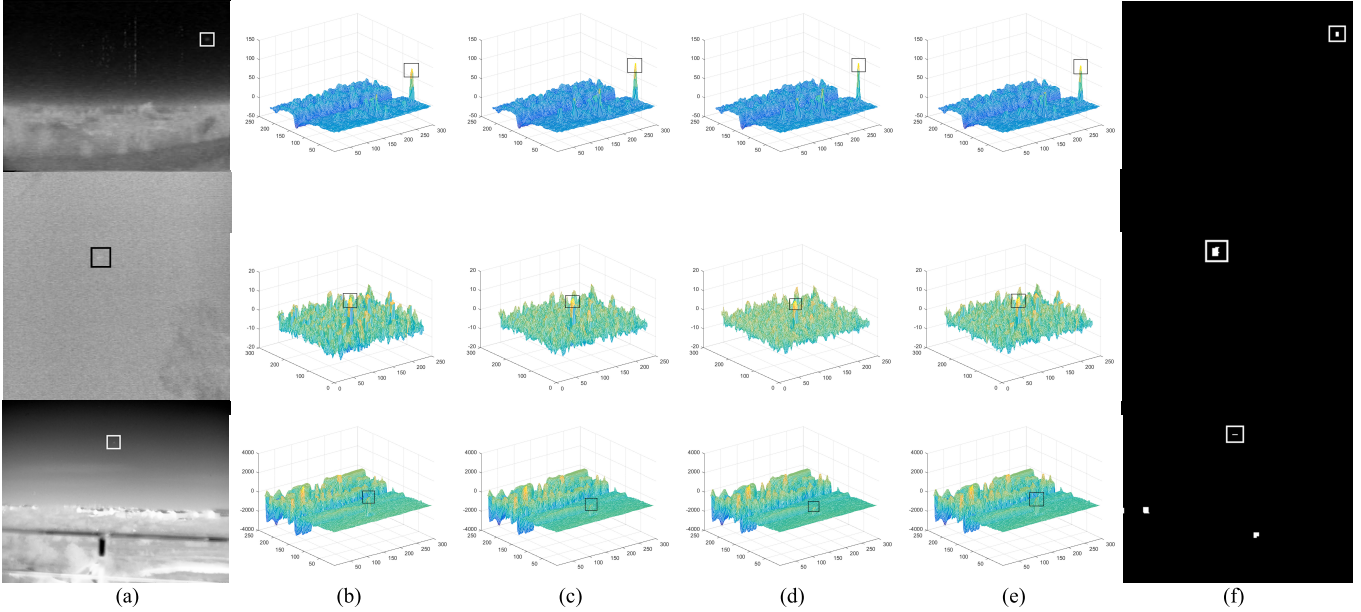


Fig. 4. (From top to bottom) Detection results using the proposed algorithm for Seq. 1, Seq. 2, and Seq. 3. (a) Raw IR image samples of the three sequences. (b) RLCM result for scale 1. (c) RLCM result for scale 2. (d) RLCM result for scale 3. (e) Final multiscale RLCM result. (f) Detection results; each connected area is regarded as a target.

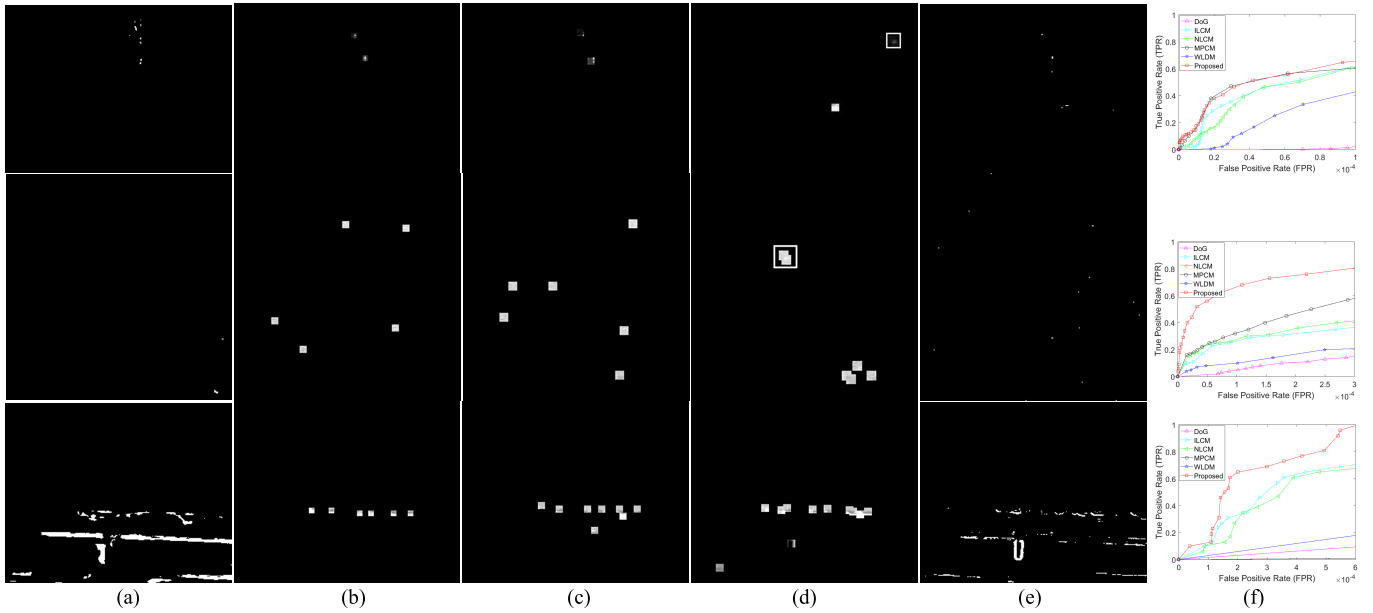


Fig. 5. Comparison of detection results between different algorithms. (From top to bottom) Detection results of Seq. 1, Seq. 2, and Seq. 3 using (a) DoG, (b) ILCM, (c) NLCM, (d) MPCM, and (e) WLDL. (f) ROC curves of different algorithms.

From Fig. 2 (middle) and considering K_1 is better to be larger than 1, we can get that for a smaller target (3×3 or 5×5), K_1 is suggested to be set from 2 to 4; for a larger target (7×7 or 9×9), K_1 is suggested to be set from 4 to 9.

Then, we set K_1 to a constant value of 2 (target size 3×3), 4 (target size 5×5), or 9 (target size 7×7 and 9×9), and tested different K_2 ; here, $K_2 = 1, 4, 9, 16, 25$ were tested. The ROC curves are shown in Fig. 2 (bottom). From Fig. 2 (bottom) and considering K_2 is better to be slightly larger than K_1 , we can get that a K_2 which is 2–7 larger than K_1 is suggested. (It is necessary to point out that the target size is usually unknown

in real applications, so multiscale detection with different K_1 and K_2 will be needed.)

The cell size N is another key parameter. Theoretically, to ensure that a cell can contain the total small target while introducing as few interferences as possible, N should be approximated to the general maximal size of small targets [11]. According to SPIE, a small target is usually smaller than 9×9 , so N is suggested to be set to about 9×9 . To verify this conclusion, we use a real IR sequence [15] which contains 400 frames to test different N , and the ROC curves are shown in Fig. 3. Here, three scales are used; (K_{1s}, K_{2s}) are (2, 4),

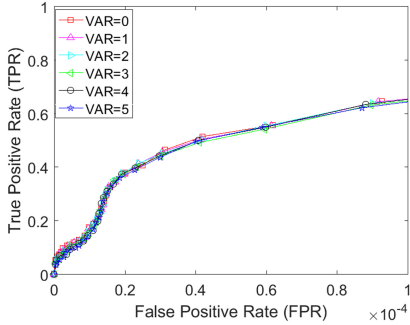


Fig. 6. ROC curves of Seq. 1 for different noise variance VAR.

(5, 9), and (9, 16) when $s = 1, 2$, and 3 , respectively. It can be easily seen that 9×9 is a proper value for N .

B. Experimental Results and Comparisons

To verify the effectiveness of the proposed algorithm, three real IR sequences had been used; Seq. 1 contains 400 frames with a 7×5 target (the same sequence used in Fig. 3), Seq. 2 contains 100 frames with a 5×5 target, and Seq. 3 contains 100 frames with a 3×3 target. The detection results are shown in Fig. 4. Here, three scales are used; (K_{1s}, K_{2s}) are $(2, 4)$, $(5, 9)$, and $(9, 16)$ when $s = 1, 2$, and 3 , respectively. N is 9×9 .

It can be seen from Fig. 4 that in the raw IR images, the targets are dim and the backgrounds are complex. After the multiscale RLCM computation, the targets are salient and complex backgrounds are suppressed. At last, the targets are correctly output while most backgrounds are discarded; only a few of false alarms emerge in Seq. 3 since Seq. 3 has a very small dim target and very complex backgrounds.

In order to further illustrate the effectiveness of the proposed algorithm, shown in Fig. 5, we give the detection results for the same images in Fig. 4 using other five state-of-the-art algorithms, including DoG [6], MPCM [9], ILCM [4], NLCM [11], and WLDM [12]. It can be seen that DoG, ILCM, NLCM, and WLDM could not detect the small targets correctly for all the three sequences; instead, a lot of false alarms emerge. MPCM, although detected the targets correctly in Seq. 1 and Seq. 2, failed to detect the target in Seq. 3. Besides, false alarms emerge in all the three sequences, too. Comparing to Fig. 4, it can be seen that the proposed algorithm can achieve the best detection performance in all the three sequences.

Fig. 5 also gives the comparisons of the detection results for each whole sequence using ROC curves. From the ROC curves, it can be seen that DoG has the worst performance since it is a difference form local contrast method and cannot enhance the small dim targets effectively. WLDM has a better performance since it is a ratio form local contrast method and can effectively enhance the dim targets; however, it cannot eliminate high brightness backgrounds effectively. ILCM and NLCM have a better performance than DoG and WLDM since they are both ratio form local contrast methods and they both using DoG as preprocessing, so targets can be enhanced and high brightness backgrounds can be eliminated. MPCM can achieve a satisfied performance in Seq. 1 and Seq. 2, but its performance in Seq. 3 is the worst, because the target is too dim and the backgrounds are too complex. The proposed algorithm can achieve the best detection performance

with good robustness in all the three sequences, since it can effectively enhance true small targets while suppressing all the other interferences simultaneously, and does not need any preprocessing algorithm.

Noise is a key influence factor; Fig. 6 gives the performances of the proposed algorithm under different levels of random noises. Seq. 1 is selected as an example here, and zero-mean Gaussian white noises with variances 1, 2, 3, 4, and 5 are added. From the ROC curves, we can get that the performance only decreases slightly after the noises are added, which means that the proposed algorithm has a good robustness against noises.

IV. CONCLUSION

In this letter, an IR small dim target detection algorithm utilizing the multiscale RLCM is proposed. It can enhance true small targets effectively and suppress all the other interferences. Experimental results show that the proposed algorithm can deal with different sizes of small targets under complex backgrounds and has a better effectiveness and robustness. Besides, the proposed algorithm has the potential of parallel processing, which is useful for improving the detection speed.

REFERENCES

- [1] C. Gao, D. Meng, Y. Yang, Y. Wang, X. Zhou, and A. G. Hauptmann, "Infrared patch-image model for small target detection in a single image," *IEEE Trans. Image Process.*, vol. 22, no. 12, pp. 4996–5009, Dec. 2013.
- [2] Y. Bi, X. Bai, T. Jin, and S. Guo, "Multiple feature analysis for infrared small target detection," *IEEE Geosci. Remote Sens. Lett.*, vol. 14, no. 8, pp. 1333–1337, Jul. 2017.
- [3] C. Yang, J. Ma, S. Qi, J. Tian, S. Zheng, and X. Tian, "Directional support value of Gaussian transformation for infrared small target detection," *Appl. Opt.*, vol. 54, no. 9, pp. 2255–2265, Mar. 2015.
- [4] J. Han, Y. Ma, B. Zhou, F. Fan, K. Liang, and Y. Fang, "A robust infrared small target detection algorithm based on human visual system," *IEEE Geosci. Remote Sens. Lett.*, vol. 11, no. 12, pp. 2168–2172, Dec. 2014.
- [5] X. Shao, H. Fan, G. Lu, and J. Xu, "An improved infrared dim and small target detection algorithm based on the contrast mechanism of human visual system," *Infr. Phys. Technol.*, vol. 55, no. 5, pp. 403–408, Sep. 2012.
- [6] X. Wang, G. Lv, and L. Xu, "Infrared dim target detection based on visual attention," *Infr. Phys. Technol.*, vol. 55, no. 6, pp. 513–521, Nov. 2012.
- [7] J. Han, Y. Ma, J. Huang, X. Mei, and J. Ma, "An infrared small target detecting algorithm based on human visual system," *IEEE Geosci. Remote Sens. Lett.*, vol. 13, no. 3, pp. 452–456, Mar. 2016.
- [8] K. Xie, K. Fu, T. Zhou, J. Zhang, J. Yang, and Q. Wu, "Small target detection based on accumulated center-surround difference measure," *Infr. Phys. Technol.*, vol. 67, pp. 229–236, Nov. 2014.
- [9] Y. Wei, X. You, and H. Li, "Multiscale patch-based contrast measure for small infrared target detection," *Pattern Recognit.*, vol. 58, pp. 216–226, Oct. 2016.
- [10] C. L. P. Chen, H. Li, Y. Wei, T. Xia, and Y. Y. Tang, "A local contrast method for small infrared target detection," *IEEE Trans. Geosci. Remote Sens.*, vol. 52, no. 1, pp. 574–581, Jan. 2014.
- [11] Y. Qin and B. Li, "Effective infrared small target detection utilizing a novel local contrast method," *IEEE Geosci. Remote Sens. Lett.*, vol. 13, no. 12, pp. 1890–1894, Dec. 2016.
- [12] H. Deng, X. Sun, M. Liu, C. Ye, and X. Zhou, "Small infrared target detection based on weighted local difference measure," *IEEE Trans. Geosci. Remote Sens.*, vol. 54, no. 7, pp. 4204–4214, Jul. 2016.
- [13] C. Wang and S. Qin, "Adaptive detection method of infrared small target based on target-background separation via robust principal component analysis," *Infr. Phys. Technol.*, vol. 69, pp. 123–135, Mar. 2015.
- [14] J. Davis and M. Goadrich, "The relationship between precision-recall and ROC curves," in *Proc. ACM 23rd Int. Conf. Mach Learn.*, 2006, pp. 233–240.
- [15] IEEE OTCBVS WS Series Bench; Roland Miezianko, Terravic Research Infrared Database. Accessed: Jul. 17, 2016. [Online]. Available: <http://vcipl-okstate.org/pbvs/bench/index.html>